Cutoff tailorability of heterojunction terahertz detectors

S. G. Matsik, M. B. M. Rinzan, and A. G. U. Perera[a)]
Department of Physics and Astronomy, Georgia State University, Atlanta, Georgia 30303

H. C. Liu, Z. R. Wasilewski, and M. Buchanan
Institute for Microstructural Sciences, National Research Council, Ottawa K1A 0R6, Canada

(Received 9 August 2002; accepted 11 November 2002)

Heterojunction interfacial work function internal photoemission (HEIWIP) detectors provide an interesting approach to the development of quantum detectors for the terahertz range. In this letter, the cutoff frequency/wavelength variation of HEIWIP detectors having different Al fractions in AlGaAs/GaAs structures is experimentally verified, and a model is presented for designing the structures. A key feature of HEIWIP responsivity is the ability to cover a broad frequency range in a single detector with cutoff tailorability by adjusting the Al fraction in the barrier regions. Extending the response to lower frequencies by the use of AlGaAs emitters and GaAs barriers is also discussed. © *2003 American Institute of Physics.* [DOI: 10.1063/1.1534409]

Although the terahertz (THz) region is of considerable interest for imaging and communications,[1,2] there are few suitable detectors operating in this region. The Si blocked impurity band detectors operate at the high frequency end of this range (>7 THz) and stressed Ge:Ga detectors can operate as low as 1.5 THz. However the stress requirements of the Ge:Ga detectors make them relatively unsuited for use in array formats. The other major alternative, bolometers, are slower than photon detectors severely curtailing their use in real time applications. In this letter, results are reported on a heterojunction interfacial work function internal photoemission (HEIWIP) detector operating in the terahertz frequency range of 3.2–15 THz (20–90 μm). Analysis shows that the response can be extended to operate up to 1 THz (300 μm).

The HEIWIP detectors which combine the free carrier absorption of the homojunction interfacial work function internal photoemission (HIWIP) detectors[3] with the material composition of quantum well infrared photodetectors (QWIPs) have been experimentally demonstrated,[4] showing improved performance compared to HIWIP[3] and QWIP[5] detectors. The typical HEIWIP detector structure consists of a p-doped GaAs emitter (absorber) region followed by an undoped AlGaAs barrier region as shown in Fig. 1. Although the structure appears similar to a p-type QWIP the emitter/absorber in a HEIWIP is thicker than the well of a QWIP forming a three-dimensional carrier distribution in HEIWIPs rather than quantized states as in a QWIP. The basic idea of HEIWIP detectors is to add the valence band offset for the GaAs/AlGaAs interface to the offset from the doping (N_A) in the emitters. The contribution from the doping (Δ_d) is the same as for HIWIPs and is found as in Ref. 6 giving ~ 9 meV for p-GaAs for doping in the range 10^{18}–10^{19} cm^{-3}. The Al fraction contribution is taken as $\Delta_{Al}=(x*530)$ meV where x is the Al fraction. The total barrier at the interface is then $\Delta=\Delta_d+\Delta_{Al}$.

The cutoff frequency (f_c) can be determined directly from $f_c=\Delta/4.133$ where f_c is in THz and Δ is in millielectron volts. The Al fraction x can be reduced to any value in theory. However a practical lower limit will be around $x \geqslant 0.005$ with $f_c \geqslant 2.7$ THz. (For $x=0$ the device will no longer be a HEIWIP, and will have a ~ 9 meV offset for $N_A=3\times10^{18}$ cm^{-3} giving $f_c=2.17$ THz.) Further decrease in f_c below 2.7 THz (i.e., beyond ~ 110 μm) will require a change in the design due to the minimum $\Delta=\Delta_d$ from the band gap narrowing. One possible approach to avoid this limit is to use AlGaAs as the emitter and GaAs as the barrier. The band gap narrowing in the doped AlGaAs will be partially offset by the increased band gap of the AlGaAs relative to the GaAs as seen in Fig. 2, giving $\Delta=\Delta_d-\Delta_{Al}$. For example, a $f_c=0.9$ THz (335 μm) detector would have an Al fraction of ~ 0.01. Based on calculations the far infrared absorption in AlGaAs is expected to be very similar to GaAs, due to the very low Al content giving performances similar to the current devices with AlGaAs barriers.

The use of a heterojunction in HEIWIPs has several advantages over the homojunction approach. (1) The ability to vary f_c while keeping the doping density (N_A) constant. This allows the doping to be adjusted to obtain the optimum combination of dark current and responsivity while not changing λ_c. (2) The effective interface in a heterojunction is sharper

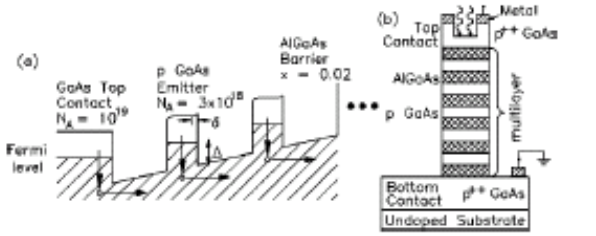

FIG. 1. (a) A partial band diagram of the top two periods for a HEIWIP detector using doped GaAs as the emitter layer and undoped AlGaAs as the barrier with the work function Δ (the difference between the barrier energy and the fermi energy) indicated. The emitter doping forms a three-dimensional carrier distribution. The device reported on has 3×10^{18} cm^{-3} Be doped 158 Å emitters and 800 Å $Al_xGa_{1-x}As$ barriers. (b) Schematic of a HEIWIP detector after processing. A window is opened on the top side for frontside illumination.

a)Author to whom correspondence should be addressed; electronic mail: uperera@gsu.edu

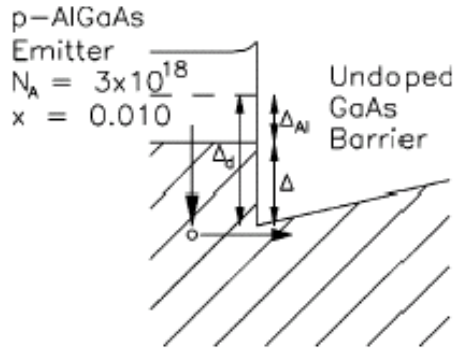

FIG. 2. Band diagram of the emitter/barrier interface for a device using doped AlGaAs as the emitter and GaAs as the barrier to extend f_c below 2.7 THz. The parameters shown are for a device with $f_c=0.9$ THz ($\lambda_c \sim 335$ μm). The dashed line in the emitter indicates the fermi level location if the emitter was GaAs. The contributions to Δ from the doping (Δ_d) and Al fraction (Δ_{Al}) are indicated by the vertical arrows. The effective barrier is $\Delta-\Delta_{Al}-\Delta_d$.

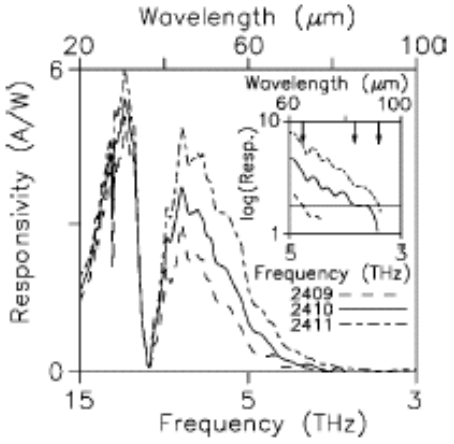

FIG. 3. Experimental responsivity spectra for 3.5 kV/cm obtained at 4.2 K. The only difference in the samples was the Al fraction which was $x=0.02$, 0.01, and 0.005 for Nos. 2409, 2410, and 2411, respectively. The data show a decrease in f_c with decreasing x. The sharp decrease near 8 THz is due to the restrahlen effect. The inset shows a log plot of the response showing the cutoff (indicated by the arrows) with $\lambda_c=65$, 84, and 92 μm for sample Nos. 2409, 2410, and 2411, respectively, showing the effect of varying x.

than in HIWIPs due to the absence of space charge effects.[7] (3) For high doping, effects of heavy-light hole transitions can limit λ_c for HIWIPs. Because the doping does not need to be as high in HEIWIPs at long λ_c this limit can be avoided.

Two important performance factors for the design of a HEIWIP detector are the spectral response and dark current. The spectral response is characterized by f_c or λ_c where the response goes to zero, the peak responsivity position (f_p or λ_p) and the peak quantum efficiency η_p. The overall goal is to maximize response while minimizing the dark current to obtain a high D^* (specific detectivity). The basic approach to calculating the responsivity for a HEIWIP detector is similar to that done previously for the HIWIP detector.[6] The difference being the origin of the barrier work function and the effect of space charge. The responsivity is given by

$$R=q\eta/hf, \tag{1}$$

where q is the electron charge, η is the total quantum efficiency of the detector, f is the frequency, and h is Planck's constant. The η is the product of the photon absorption efficiency and the internal quantum efficiency (the probability that photoexcited carriers undergo internal photoemission) $\eta=\eta_a\eta_t$. Here the collection efficiency is assumed to be 1 since the maximum barrier height is at the interface due to the absence of space charge effects so that any carriers scattered after internal photoemission will be collected.

The η_a of a single layer is $\eta_a=(F/F_0)^2[1-\exp(-\alpha W)]$ where α is the wavelength dependent absorption coefficient, W is the emitter layer thickness, F is the optical electric field in the emitter layer, and F_0 is the optical electric field incident on the device. The factor $(F/F_0)^2$ involving the electric fields adjusts for any resonance effects in the device structure, reflection at the top surface, etc., which can be determined as in Ref. 8. For high frequency operation resonant cavity effects can be significant. For $f>38$ THz (8 μm), the absorption is a combination of free carrier and intersubband absorptions[9] that varies as $1/f^2$ and is nearly independent of frequency below 38 THz (>8 μm). The η_t can be calculated using the same model used for HIWIPs[6] with Δ replaced by the HEIWIP value. The η_t is zero at f_c and increases continually with frequency.

The primary factors in determining the responsivity of a detector are Δ, N_A, and W. In practice since R is typically calculated numerically the peak response is determined from a plot of R vs λ. The primary factor in determining the spectral shape will be the value of Δ chosen for the detector if cavity effects[8,10] are not included. If the optical electric field strength is constant in the device (ignoring the resonant cavity effect), the high frequency end of the response is independent of x as η_t becomes almost constant. The slope of low frequency response region depends weakly on x. As a result f_p and f_c (λ_p and λ_c) will vary by the same factor as Δ is increased. In devices for which the cavity effect is significant the peak response can be shifted significantly from the noncavity case. Maximum peak response R_p occurs when the device thickness causes the cavity peak to match the position predicted from the noncavity response curve. Designing the cavity peak to be near (but not at) the noncavity response peak will produce a broader response but with a reduced R_p. The magnitude of the response can be increased by increasing (1) the doping, (2) the thickness, and (3) the number of emitter layers. There is a practical limit to increasing the emitter doping density due to corresponding increases in the dark current. In addition having the doping

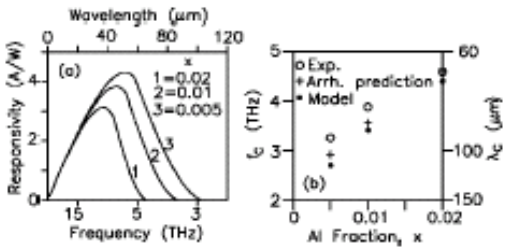

FIG. 4. (a) Calculated spectra for 150 A, 3×10^{18} cm^{-3} p-doped GaAs emitter with $Al_xGa_{1-x}As$ barrier forming a single layer detector with the electric field of 1000 V/cm for different x corresponding to the experimental samples. (b) The variation in f_c with x showing a comparison of the spectral cutoff, the cutoff predicted from the Arrhenius plot and the model result. The discrepancy between the experimental and predicted results is probably due to small variations in Δ_d.

TABLE I. Predicted and measured barrier heights, cutoff frequencies, and wavelengths from the model, Arrhenius plots, and the spectra for the three samples showing the variation with the Al fraction in the barriers. The small variation between the model and spectral values is probably due to small deviations of the actual parameters from the design values.

Sample No.	Δ_{spec} (meV)	Δ_{Arrh} (meV)	Δ_{model} (meV)	f_{spec} (THz)	f_{Arrh} (THz)	f_{model} (THz)	λ_{spec} (μm)
2409	19.0 ± 0.1	19 ± 0.2	19.6	4.6 ± 0.1	4.6 ± 0.1	4.4	65 ± 1
2410	15.0 ± 0.1	14.5 ± 0.2	14.3	3.9 ± 0.1	3.5 ± 0.1	3.3	84 ± 1
2411	13.4 ± 0.1	12 ± 0.2	11.6	3.6 ± 0.1	2.9 ± 0.1	2.7	92 ± 1

density in a region where the band gap narrowing is a weak function of it should improve uniformity in the devices. The optimum emitter thickness (and number of layers) can be determined by maximizing the device response. For a single emitter layer structure the optimum thickness is ~700 Å, while for multilayer structures (>20 layers) the optimum thickness of the individual emitter layers is reduced to 150–250 Å. For example, a 3-μm-thick detector with 1000-Å-thick barriers would be optimized with 26 layers with 153-Å-thick emitters. To obtain the optimum thickness for multilayer structures, the device thickness is determined to obtain the desired resonant cavity enhancement and the barrier thickness is determined to reduce the tunneling current to the desired level. With these two values fixed the number of layers and the associated emitter thickness are then optimized.

The device structures tested contained 30 periods of 3×10^{18} cm^{-3} Be doped 158 Å GaAs emitters (W) and 800 Å $Al_xGa_{1-x}As$ barriers as shown in Fig. 1 giving 31 emitters with the etched top contact acting as an emitter. The Al fraction was varied, with $x=0.02$, 0.01 and 0.005 ($D=18$, 13.5, and 11.2 meV) for sample Nos. 2409, 2410, and 2411, respectively, to adjust f_c. The top and bottom contacts were Be doped to 1×10^{19} cm^{-3} with thicknesses 0.2 and 0.7 μm, respectively. The devices were fabricated as before.[4] Normal incidence radiation can be absorbed unlike in QWIPs allowing simple coupling for incoming radiation.

The responsivity was measured using a Fourier-transform infrared spectrometer with a Si composite bolometer as a reference detector. The experimental spectra for all three samples at 3.5 kV/cm for 4.2 K are shown in Fig. 3 with a strong response for frequencies higher than 6 THz. The inset shows the raw response normalized so that the response was 1 at the frequency where the signal equaled the noise determined from the deviation of multiple measurements. The cutoff values were $f_c=4.6\pm0.1$, 3.9 ± 0.1, and 3.6 ± 0.1 THz (65, 84, and 92 μm) for sample Nos. 2409, 2410, and 2411, respectively, as indicated by the arrows. The responsivity at 10 THz (30 μm) was ~5.6 A/W for sample Nos. 2409 and 2410 and 6.0 A/W for 2411. The expected f_p is near 8 THz ($\lambda=42.5$ μm); but this is concealed by absorption in the restrahlen region, so the peak variation with x could not be observed for these samples. The η was 22% for Nos. 2409 and 2410 and 25% for No. 2411 at 10 THz (30 μm). The slight difference in response between the samples is probably due to a combination of the resonant cavity effect and the strong drop in absorption in the restrahlen region. The noise current of the detectors was measured using a spectrum analyzer giving $S_I\sim2.7\times10^{-23}$ A^2/Hz for 2409 and 2410 and $S_I\sim3.2\times10^{-23}$ A^2/Hz for 2411. The resulting D^* was 4×10^{10} Jones (cm $\sqrt{\text{Hz}}$/W) for Nos. 2409 and 2410 and 3.6×10^{10} Jones for No. 2411 at 4.2 K. Calculated single layer responsivities will be lower than the experimental responsivities for multilayer samples as seen in Fig. 4(a). The experimental data show increased response at low frequency with decreased Al fraction while the high frequency region showed similar response for all three samples.

The observed f_c as well as the values predicted from a modified Arrhenius plot of dark current variation with temperature and the model for the three samples are shown in Fig. 4(b) and Table I with f_c decreasing as x decreases. The difference in the experimental and model values corresponds to a variation of 1–2 meV in the barrier height which may be due to the deviation of the band gap narrowing. There is also a small difference between the spectral and Arrhenius values for f_c that is probably due to inelastic scattering of photoexcited carriers before emission.[11]

In conclusion, a model which can be used to design HEIWIP detectors is presented giving good results at low frequencies and providing a good starting point for device design. Further studies on the details of the carrier escape process should improve the model in the high frequency range. Based on the model detectors with different Al fractions were fabricated and the predicted variation in f_c was observed.

This work was supported in part by the NSF under Grant No. ECS-0140434. M. B. M. Rinzan is supported by GSU RPE funds. The work at NRC is supported in part by DND.

[1] M. Herrmann, M. Tani, and K. Sakai, J. Appl. Phys. **91**, 1247 (2002).
[2] M. S. Sherwin, Proc. SPIE **3617**, 58 (1999).
[3] W. Z. Shen, A. G. U. Perera, H. C. Liu, M. Buchanan, and W. J. Schaff, Appl. Phys. Lett. **71**, 2677 (1997).
[4] A. G. U. Perera, S. G. Matsik, B. Yaldiz, H. C. Liu, A. Shen, M. Gao, Z. R. Wasilewski, and M. Buchanan, Appl. Phys. Lett. **78**, 2241 (2001).
[5] A. G. U. Perera, W. Z. Shen, S. G. Matsik, H. C. Liu, M. Buchanan, and W. J. Schaff, Appl. Phys. Lett. **72**, 1596 (1998).
[6] A. G. U. Perera, H. X. Yuan, and M. H. Francombe, J. Appl. Phys. **77**, 915 (1995).
[7] H. X. Yuan and A. G. U. Perera, J. Appl. Phys. **79**, 4418 (1996).
[8] A. L. Korotkov, A. G. U. Perera, W. Z. Shen, H. C. Liu, and M. Buchanan, Solid-State Electron. **45**, 87 (2001).
[9] M. L. Huberman, A. Ksendzov, A. Larsson, R. Terhune, and J. Maserjian, Phys. Rev. B **44**, 1128 (1991).
[10] A. L. Korotkov, A. G. U. Perera, W. Z. Shen, J. Herfort, K. H. Ploog, W. J. Schaff, and H. C. Liu, J. Appl. Phys. **89**, 3295 (2001).
[11] F. D. Shepherd, Proc. SPIE **1735**, 250 (1992).